Int. J. Heat Mass Transfer. Vol. 27, No. 1, pp. 1–13, 1984
Printed in Great Britain

0017 9310/84 $3.00 + 0.00

TOTAL HEMISPHERICAL EMITTANCES FOR CO_2 OR H_2O INCLUDING PARTICULATE SCATTERING

R. D. SKOCYPEC and R. O. BUCKIUS
Department of Mechanical and Industrial Engineering, University of Illinois at Urbana-Champaign, Urbana, IL 61801, U.S.A.

(*Received* 15 *September* 1982 *and in final form* 15 *March* 1983)

Abstract—The total hemispherical emittance from a planar layer containing a spectrally absorbing gas and isotropically scattering particulate is determined. The exponential wide band model is used to represent the gaseous absorption while the optical path length concept is employed to include the effects of scattering. Total emittance values for either water vapor or carbon dioxide with particulate are presented. Numerous gas-scattering interactive effects and variable effects are identified and explained. A charted solution technique is presented which allows approximate yet accurate total emittance values to be obtained without calculation.

NOMENCLATURE

- A_{i^*} wide band absorptance for band i
- C correction factor, defined in equation (24)
- f blackbody fraction function
- i intensity
- L length
- N total number of bands
- P reflectance path length distribution function, pressure
- P_A absorbing gas partial pressure
- P_AL product of absorbing gas partial pressure and path length
- Q heat flux path length distribution function
- q radiative heat flux
- T transmittance path length distribution function, temperature
- y geometric depth perpendicular to layer surface.

Greek symbols

- α absorption coefficient
- α_b integrated band intensity parameter
- γ $\alpha_v/(\alpha_S+\sigma)$
- ε emittance
- ε_{i^*} wide band emittance for band i
- η_b pressure broadening parameter
- κ optical depth
- κ_{HL} optical depth at band head or center
- κ_S $(\alpha_S+\sigma)y$
- λ optical path length
- $\langle\lambda\rangle$ mean optical path length
- ν wavenumber
- ρ reflectance
- ρ_{i^*} wide band reflectance for band i
- σ scattering coefficient, Stefan–Boltzmann constant
- τ transmittance
- τ_{i^*} wide band transmittance for band i
- ω_b band width parameter
- ω_S scattering albedo $[=\sigma/(\alpha_s+\sigma)]$.

Superscripts

- $+$ positive direction
- $-$ negative direction.

Subscripts

- b blackbody
- G gas quantity
- i evaluated at band i
- L evaluated at the total perpendicular layer depth
- l lower
- ν wavenumber dependent quantity
- S scattering quantity
- T total quantity
- u upper
- * dimensionless quantity

INTRODUCTION

NUMEROUS heat transfer problems require the analysis of radiative transfer within a medium containing molecular gases and particulate. The molecular gases absorb and emit in a very spectrally dependent fashion while the particulate absorb and emit as well as scatter radiant energy. Both constituents have received considerable attention separately although a complete analysis of the composite medium has been lacking. The results of this analysis are certainly applicable to energy conversion systems such as furnaces, combustors and engines, in which hot combustion gases are accompanied by solid by-products of ash and soot. The radiative transfer from plumes containing metallic oxides, such as those trailing solid propellant rockets, can be determined. Additional applications include evaluating the heat transfer from fires and smokes, luminous flames and coal dust flames. The significance of the effect of the solids on the heat transfer is readily evaluated. The method of analysis is adaptable to evaluating the radiative transfer from any high temperature industrial process involving real gases and particulate.

The total emittance charts by Hottel [1] are very useful to obtain real gas emittance values. Based on experimental data, the charts have been found to be quite accurate except in regions outside the experimental domain requiring extrapolation. Since charted results do not easily lend themselves to numerical computations, many models of real gas

emission have arisen. Some, such as the narrow band models [2], maintain reasonable physical detail at the expense of prohibitively large computation time while others, such as the weighted sum of gray gases models [3], may attain reasonable accuracy with simple execution by eliminating the true detail of gaseous emission. A third technique, the exponential wide band model [4, 5], maintains the spectral nature and reduces the necessary computation by grouping the absorption lines into wider bands whose shape, size and position are thereby represented. The gray emittance from a layer of pure scattering particulate has also been considered. Both isotropic [6] and anisotropic [7] scattering have been investigated. Taylor and Foster [8] used empirical absorption coefficients to model the soot emission in luminous flames by a multiple gray gases scheme.

Work has also been performed on combined real gas and particulate emission [8–10] although no heat transfer analysis has been undertaken which includes real gas-scattering interactions on a fundamental basis. Felske and Tien [9] restricted their analysis to the small particle Rayleigh limit of Mie theory and, although emission by the particulate was included, redistribution of radiant energy by particulate scattering was therefore neglected. The deviation of their analytic results from experimental data was attributed to the neglect of scattering effects. Other works have treated particulate similarly by adding an additional absorption term [10].

The purpose of this investigation is twofold. First, to determine the total hemispherical emittance from a complete yet simple analytical basis incorporating real gas effects with the exponential wide band model and including all scattering effects by the photon path length concept [11]. In essence, Hottel's charts are extended to include scattering particulate. Particular attention is paid to gas-scattering interactive effects. The second objective is to provide simple yet accurate charted solutions with a wide range of application, which allow approximate total emittance values to be obtained without calculation.

ANALYSIS AND SOLUTION

The system of interest is composed of an isothermal homogeneous planar layer at temperature T with transparent boundaries at $\kappa = 0$ and κ_L. Both the gas and particulate are assumed to have temperature T. If the layer is nonisothermal, it may be possible to utilize a wide band scaling approximation [4] although this has not been considered in this work. The nongray absorption is due to the existence of a gaseous constituent, either CO_2 or H_2O in this work, and thus is banded. Three parameters per band, the effective broadening parameter η_b, the integrated band intensity α_b and the exponential decay width ω_b, are required to describe the gaseous absorption by the exponential wide band model [4] in terms of the dimensionless band absorption, $A_{i*}(\kappa_{HL}, \eta_b)$. The optical depth at the head or center of band i is κ_{HL}. All three parameters are generally functions of temperature and η_b is also dependent on pressure. The scattering components are assumed to absorb and scatter energy independent of wavenumber and therefore are gray. Isotropic scattering is assumed for all scattering constituents, which have an optical depth denoted as $\kappa_S = (\alpha_S + \sigma)y$ with a scattering albedo of $\omega_S = \sigma/(\alpha_S + \sigma)$. The effect of anisotropic scattering particulate can be analyzed by scaling κ_{SL} and ω_S as indicated in ref. [12]. The layer has a scattering optical thickness of $\kappa_{SL} = (\alpha_S + \sigma)L$. The spectral heat flux at optical depth κ_S, $q_\nu^{\pm}(\kappa_S, \kappa_{SL}, \omega_S, \gamma)$, includes the spectral gaseous absorption, which is parameterized by $\gamma = \alpha_\nu/(\alpha_S + \sigma)$.

The spectral heat flux must be integrated over all wavenumbers to obtain the total value. The total heat flux exiting the layer at $\kappa_S = 0$ is

$$q^-(0, \kappa_{SL}, \omega_S, \gamma) = \int_0^\infty q_\nu^-(0, \kappa_{SL}, \omega_S, \gamma)\,d\nu. \quad (1)$$

Adding and subtracting the spectral heat flux resulting from the particulate alone yields

$$q^-(0, \kappa_{SL}, \omega_S, \gamma) = \int_0^\infty q_\nu^-(0, \kappa_{SL}, \omega_S, 0)\,d\nu - \int_0^\infty [q_\nu^-(0, \kappa_{SL}, \omega_S, 0) - q_\nu^-(0, \kappa_{SL}, \omega_S, \gamma)]\,d\nu. \quad (2)$$

The first integral represents the emission from the particulate and is expressed in terms of the emittance for the scattering constituents. The second integral includes the banded gaseous contribution. The integrand goes to zero outside the banded regions and, assuming that the Planck function evaluated at the band head or center is a constant over the banded region, the second integral is represented as a sum over N bands. Equation (2) becomes [13]

$$\varepsilon_T(\kappa_{SL}, \omega_S, T, P_A L) = \frac{q^-(0, \kappa_{SL}, \omega_S, \gamma)}{\sigma T^4} = \varepsilon_S(\kappa_{SL}, \omega_S) - \sum_{i=1}^{N} \frac{\pi i_{\nu_i b}(T)}{\sigma T^4} \times \omega_{bi}\varepsilon_{i*}(\kappa_{SL}, \omega_S, \kappa_{HLi}, \eta_{bi}), \quad (3)$$

where the total emittance is shown to have a direct dependence on $P_A L$ and T, since, for a given absorbing gas and total pressure, the wide band parameters are functions only of $P_A L$ and T. The term $\varepsilon_S(\kappa_{SL}, \omega_S)$ is the total hemispherical gray emittance of the particulate which absorbs and scatters and is given by

$$\varepsilon_S(\kappa_{SL}, \omega_S) = \frac{1}{\sigma T^4} \int_0^\infty q_\nu^-(0, \kappa_{SL}, \omega_S, 0)\,d\nu. \quad (4)$$

The gaseous contribution from a single band is given by

$$\varepsilon_{i*}(\kappa_{SL}, \omega_S, \kappa_{HL}, \eta_b) = \frac{1}{\pi i_{\nu_i b}(T)} \int_0^\infty [q_\nu^-(0, \kappa_{SL}, \omega_S, 0) - q_\nu^-(0, \kappa_{SL}, \omega_S, \gamma)]\,d\left(\frac{\nu}{\omega_b}\right). \quad (5)$$

The difference between the total heat flux with only gray scattering constituents and the total heat flux with both gray and band absorption in equation (5) can be expressed in terms of the transmittance and reflectance. For a boundary source problem with the medium having no emission, the hemispherical spectral reflectance and transmittance are defined in terms of the radiative heat flux which exits the layer at $\kappa_S = 0$ and κ_{SL}, respectively, and are denoted as

$$\rho_\nu(\kappa_{SL}, \omega_S, \gamma) = \frac{q_\nu^-(0, \kappa_{SL}, \omega_S, \gamma)}{\pi i_{\nu b}(T)}, \quad (6)$$

and

$$\tau_\nu(\kappa_{SL}, \omega_S, \gamma) = \frac{q_\nu^+(\kappa_{SL}, \kappa_{SL}, \omega_S, \gamma)}{\pi i_{\nu b}(T)}. \quad (7)$$

The hemispherical spectral emittance for an isothermal layer at T with no boundary incidence is given by an energy balance as

$$\varepsilon_\nu(\kappa_{SL}, \omega_S, \gamma) + \rho_\nu(\kappa_{SL}, \omega_S, \gamma) + \tau_\nu(\kappa_{SL}, \omega_S, \gamma) = 1. \quad (8)$$

Expressions for the total heat flux exiting the medium for a single wide band are also written in terms of the reflectance and transmittance. Termed hemispherical wide band quantities [13], expressions for reflectance and transmittance are defined as

$$\rho_{i*}(\kappa_{SL}, \omega_S, \kappa_{HL}, \eta_b) = \int_0^\infty [\rho_\nu(\kappa_{SL}, \omega_S, 0) - \rho_\nu(\kappa_{SL}, \omega_S, \gamma)] \, d\left(\frac{\nu}{\omega_b}\right), \quad (9)$$

and

$$\tau_{i*}(\kappa_{SL}, \omega_S, \kappa_{HL}, \eta_b) = \int_0^\infty [\tau_\nu(\kappa_{SL}, \omega_S, 0) - \tau_\nu(\kappa_{SL}, \omega_S, \gamma)] \, d\left(\frac{\nu}{\omega_b}\right). \quad (10)$$

The hemispherical wide band emittance for an isothermal layer given in equation (5) is correspondingly obtained from the reflectance and transmittance quantities as

$$\begin{aligned}\varepsilon_{i*}(\kappa_{SL}, \omega_S, \kappa_{HL}, \eta_b) &= \int_0^\infty [\varepsilon_\nu(\kappa_{SL}, \omega_S, 0) - \varepsilon_\nu(\kappa_{SL}, \omega_S, \gamma)] \, d\left(\frac{\nu}{\omega_b}\right) \\ &= -\rho_{i*}(\kappa_{SL}, \omega_S, \kappa_{HL}, \eta_b) - \tau_{i*}(\kappa_{SL}, \omega_S, \kappa_{HL}, \eta_b), \end{aligned} \quad (11)$$

where equations (8)–(10) have been utilized. Therefore, equation (3) is alternately represented as

$$\begin{aligned}\varepsilon_T(\kappa_{SL}, \omega_S, T, P_A L) &= \varepsilon_S(\kappa_{SL}, \omega_S) + \sum_{i=1}^{N} \frac{\pi i_{\nu_i b}(T)}{\sigma T^4} \\ &\times \omega_{bi}[\rho_{i*}(\kappa_{SL}, \omega_S, \kappa_{HLi}, \eta_{bi}) \\ &+ \tau_{i*}(\kappa_{SL}, \omega_S, \kappa_{HLi}, \eta_{bi})]. \end{aligned} \quad (12)$$

Exact analysis

The optical path length concept is utilized to obtain $\rho_{i*}(\kappa_{SL}, \omega_S, \kappa_{HL}, \eta_b)$ and $\tau_{i*}(\kappa_{SL}, \omega_S, \kappa_{HL}, \eta_b)$ [14]. The optical path length distribution functions $Q^\pm(\lambda, \omega_S\kappa_S, \omega_S\kappa_{SL})\,d\lambda$, $P(\lambda, \omega_S\kappa_{SL})\,d\lambda$ and $T(\lambda, \omega_S\kappa_{SL})\,d\lambda$ are viewed as probabilities that a photon which traverses an optical path length between λ and $\lambda + d\lambda$ contributes to the radiative heat flux, reflectance and transmittance, respectively. The distributions are defined so that when integrated over the entire λ domain, they are equivalent to the radiative heat flux, reflectance and transmittance, respectively, in a conservative medium ($\omega_S = 1$). The arguments $\omega_S\kappa_S(=\sigma y)$ and $\omega_S\kappa_{SL}(=\sigma L)$ are used since the path length distribution functions are results for a conservative medium. The radiative heat flux for a gray nonconservative scattering medium is expressed as

$$q_\nu^\pm(\kappa_S, \kappa_{SL}, \omega_S, \gamma = 0) = \int_0^\infty e^{-(1/\omega_S - 1)\lambda} Q^\pm(\lambda, \omega_S\kappa_S, \omega_S\kappa_{SL})\,d\lambda. \quad (13)$$

Defining the spectral reflectance and transmittance in terms of the optical path length distributions yields

$$\rho_\nu(\kappa_{SL}, \omega_S, \gamma = 0) = \int_0^\infty e^{-(1/\omega_S - 1)\lambda} P(\lambda, \omega_S\kappa_{SL})\,d\lambda, \quad (14)$$

and

$$\tau_\nu(\kappa_{SL}, \omega_S, \gamma = 0) = \int_0^\infty e^{-(1/\omega_S - 1)\lambda} T(\lambda, \omega_S\kappa_{SL})\,d\lambda, \quad (15)$$

where $P(\lambda, \omega_S\kappa_{SL})$ and $T(\lambda, \omega_S\kappa_{SL})$ are equivalent to $Q^-(\lambda, 0, \omega_S\kappa_{SL})$ and $Q^+(\lambda, \omega_S\kappa_{SL}, \omega_S\kappa_{SL})$ divided by π, respectively, corresponding to a system with diffuse unit incident intensity at $\kappa_S = 0$ and a transparent boundary at $\kappa_S = \kappa_{SL}$. Thus, with equation (8)

$$\varepsilon_S(\kappa_{SL}, \omega_S) = 1 - \int_0^\infty e^{-(1/\omega_S - 1)\lambda} [P(\lambda, \omega_S\kappa_{SL}) + T(\lambda, \omega_S\kappa_{SL})]\,d\lambda. \quad (16)$$

The photon path length distribution functions are used to easily include the effect of the spectral gaseous absorption. Note that the absorption is viewed as a depletion of an existing photon path length contribution by an amount dependent upon the absorption at the specified wavenumber under consideration. Thus, the hemispherical wide band reflectance and transmittance quantities for both gray and spectral absorption in the medium become

$$\rho_{i*}(\kappa_{SL}, \omega_S, \kappa_{HL}, \eta_b) = \int_0^\infty e^{-(1/\omega_S - 1)\lambda} P(\lambda, \omega_S\kappa_{SL}) A_{i*}(\kappa_{HL}\lambda/\kappa_{SL}, \eta_b)\,d\lambda, \quad (17)$$

and

$$\tau_{i*}(\kappa_{SL}, \omega_S, \kappa_{HL}, \eta_b) = \int_0^\infty e^{-(1/\omega_S - 1)\lambda} T(\lambda, \omega_S\kappa_{SL}) A_{i*}(\kappa_{HL}\lambda/\kappa_{SL}, \eta_b)\,d\lambda, \quad (18)$$

where κ_{HL} is the optical depth at band head for a strictly gaseous layer. Closed-form representations of $P(\lambda, \omega_S\kappa_{SL})$ and $T(\lambda, \omega_S\kappa_{SL})$ have been presented in ref. [11]. Once the expression for the wide band absorption is chosen, the total hemispherical emittance is obtained by equation (12), after performing the direct integrations in equations (17) and (18) with the known photon path length distributions.

The exponential wide band model as developed by Edwards and co-workers [4, 5] is used to evaluate the radiative gas properties. Model parameters for carbon dioxide and water vapor, among others, have been presented [4, 5]. Modak [15] recommended alternate parameters for the pure rotational band of water vapor with all remaining band parameters taken from Edwards. The alternate parameters are adopted in this investigation. Although Modak used the single band absorptance equation of Felske and Tien [16] in his work, the original four region expression of Edwards is used in this endeavor due to better comparisons with total gas emittance values when the original expression is employed with the reported parameters.

For multi-band problems including only molecular gases, two methods of determining total gas emittance values are possible. A simple summation over all bands is feasible, although band overlap is not recognized. The resulting expression is [4]

$$\varepsilon_G(T, P_AL) = \sum_{i=1}^{N} \frac{\pi i_{\nu_i b}(T)}{\sigma T^4} \omega_{bi} A_{i*}(\kappa_{HLi}, \eta_{bi}). \quad (19)$$

A preferable method, especially applicable to gas mixtures or wide-banded gases such as water vapor, is the block calculation procedure. Knowing the band absorption, a transmittance for each band is designated as

$$\tau_{G,i}(\kappa_{HL}, \eta_b) = [\kappa_{HL}/A_{i*}(\kappa_{HL}, \eta_b)] \times \mathrm{d}A_{i*}(\kappa_{HL}, \eta_b)/\mathrm{d}\kappa_{HL} \leqslant 0.90, \quad (20)$$

where the smaller of $\tau_{G,i}(\kappa_{HL}, \eta_b)$ and 0.90 is taken as the transmittance value. The band width is defined as

$$\Delta\nu_i = \omega_b A_{i*}(\kappa_{HL}, \eta_b)/[1 - \tau_{G,i}(\kappa_{HL}, \eta_b)]. \quad (21)$$

Whenever bands overlap, a new effective band is created with a transmittance equivalent to the product of the two original band transmittance values. The gas emittance becomes

$$\varepsilon_G(T, P_AL) = \sum_i [1 - \tau_{G,i}(\kappa_{HLi}, \eta_{bi})] \times [f(T, \nu_{li}) - f(T, \nu_{ui})], \quad (22)$$

where the summation is over all gas bands, including the effective bands created, and ν_{li} and ν_{ui} represent the lower and upper limit of band i, respectively, in terms of wavenumber.

Recognizing that band overlap is not included in the calculation of $\varepsilon_T(\kappa_{SL}, \omega_S, T, P_AL)$ by equations (12), (17) and (18), the block calculation method is utilized to determine the total emittance. Comparing equations (19) and (22) and substituting for $A_{i*}(\kappa_{HL}, \eta_b)$ in equations (17) and (18), the expression for $\varepsilon_T(\kappa_{SL}, \omega_S, T, P_AL)$ becomes

$$\varepsilon_T(\kappa_{SL}, \omega_S, T, P_AL) = \varepsilon_S(\kappa_{SL}, \omega_S) + \int_0^\infty e^{-(1/\omega_S - 1)\lambda}[P(\lambda, \omega_S\kappa_{SL}) + T(\lambda, \omega_S\kappa_{SL})] \times \sum_i [1 - \tau_{G,i}(\kappa_{HLi}\lambda/\kappa_{SL}, \eta_{bi})][f(T, \nu_{li}) - f(T, \nu_{ui})]\,\mathrm{d}\lambda, \quad (23)$$

where the summation is over all gas bands as above.

Charted solutions

The total emittance charts for H_2O and CO_2 presented by Hottel [1] are very convenient and useful in real gas radiation calculations. The exact analysis presented in the previous section incorporates scattering into real gas radiation problems. In the same vein as Hottel's charts, an approach is developed to include scattering in the form of charts.

The total hemispherical emittance of an emitting layer, for which the total pressure is maintained constant, is dependent upon four variables, those being the scattering optical depth κ_{SL} and albedo ω_S, and the gas temperature T and partial pressure and path length product P_AL. To more easily understand and present results which span the domains of these variables, a correction factor, C, is adopted and expressed as

$$C = [\varepsilon_T(\kappa_{SL}, \omega_S, T, P_AL) - \varepsilon_S(\kappa_{SL}, \omega_S)]/\varepsilon_G(T, P_AL), \quad (24)$$

so that

$$\varepsilon_T(\kappa_{SL}, \omega_S, T, P_AL) = \varepsilon_S(\kappa_{SL}, \omega_S) + C \cdot \varepsilon_G(T, P_AL), \quad (25)$$

where $\varepsilon_S(\kappa_{SL}, \omega_S)$ is the equivalent emittance of a layer containing no spectral gaseous absorption but which has identical values of the scattering parameters, and $\varepsilon_G(T, P_AL)$ is the equivalent emittance from a layer containing no scattering particulate but which has identical values of the gas parameters. The reason for defining C by equation (24) is appreciated by comparing equations (25) and (3) and noting that C, in effect, accounts for the detailed interaction of gaseous absorption and scattering. Thus, one can quickly determine the effect of particulate-spectral absorption interactions on the emittance and identify areas where scattering or gaseous contributions dominate.

As will be shown in the following section, the factor C, as defined by equation (24), is a very useful parameter. It is still a function of the four variables but the functional dependence is very smooth. The scattering variables are reduced by one by using the combination $(1 - \omega_S)\kappa_{SL}$ which has been suggested by other work [17]. The resulting charts enable accurate and quick evaluation of the total hemispherical emittance for gaseous and particulate systems.

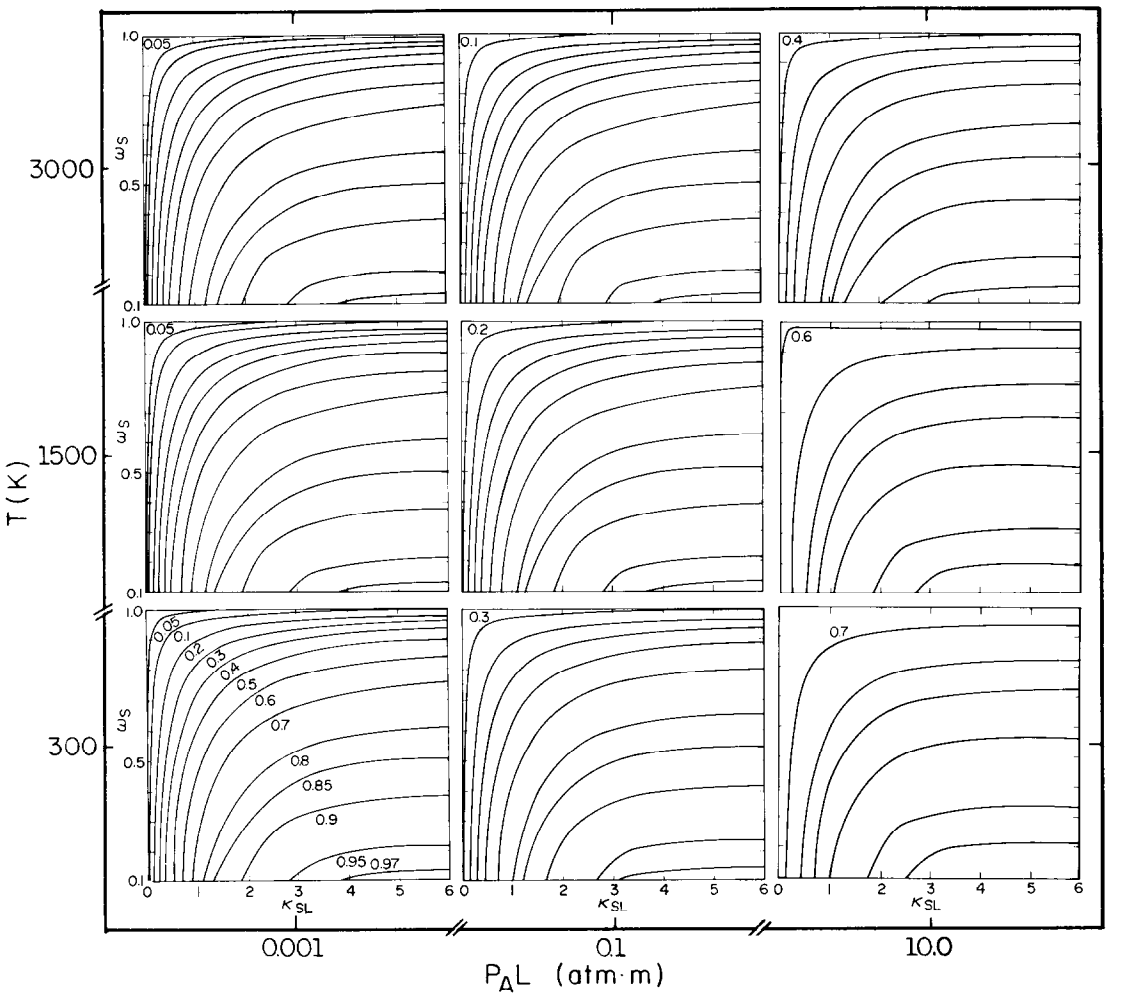

FIG. 1. Total hemispherical emittance isopleths for H_2O. Values increase from the indicated quantity in the order: 0.05, 0.1, 0.2, 0.3, 0.4, 0.5, 0.6, 0.7, 0.8, 0.85, 0.9, 0.95, 0.97.

RESULTS AND DISCUSSION†

All results presented employ the block calculation method to determine the total and gas emittance values at a total pressure of 1 atm. The application of the results to other P_T values is discussed at the end of this section. The results differ from the non-block calculation method only for water vapor at low temperatures where the extremely wide rotational band has a large influence. Modak [15] has indicated that at 300 K, 80% of the gaseous emission by water vapor is due to the rotational band.

The pure gas emittance for H_2O and CO_2 is shown in Appendix A as Figs. A1 and A2, respectively. The partial pressure of the absorbing species, P_A, is maintained at the zero limit since the emittance is influenced in a more complex manner by P_A and P_T when P_A is nonzero for H_2O. Thus, to correlate the results the limit of $P_A \to 0$ is taken, as has been presented in Hottel's charts and others. Although the effect of nonzero P_A is not great for CO_2, the limit of $P_A \to 0$ is also taken for uniformity.

† The parenthetical information for ε_T, ε_G, and ε_S are not explicitly denoted for clarity.

The pure scattering emittance is shown in Fig. A3 of Appendix A for $\omega_S \neq 1$, since the nonabsorbing case of unity albedo requires $\varepsilon_S(\kappa_{SL}, \omega_S = 1) = 0$. As either κ_{SL} increases or ω_S decreases, ε_S intensifies due to a rise in gray absorption and thus re-emission. The emittance is highly nonlinear with respect to large ω_S.

Exact results

The effects of the four variables upon which the total hemispherical emittance depends are somewhat complex, with a large degree of gas-scattering interaction. Gas effects dominate in certain regions while scattering effects prevail in other areas. Figures 1 and 2 present the total hemispherical emittance as isopleths, or constant ε_T curves, over the domains $0.1 \leqslant \omega_S < 1.0$ and $0.0 < \kappa_{SL} \leqslant 6.0$ for the particular gas parameter values indicated. From Fig. 1 for low P_AL, the effect of T is observed only at low temperatures and small ε_T values. By comparing the $T = 300$ and 1500 K graphs maintaining constant values of the scattering variables, it is seen that as T increases ε_T diminishes, and a gradual shift in isopleth position occurs as the isopleth values become smaller. However, all total emittances greater than 0.95 remain unchanged

due to dominant scattering which eliminates the temperature dependence. Negligible T effects are seen for κ_{SL} larger than 4.0. By progressing to larger P_AL values, the gas effect on the total emittance is enhanced and not only is the effect of T larger but it also occurs for all κ_{SL} presented. For $T = 300$ K, an augmentation of ε_T occurs as P_AL increases and is very large and evident at all κ_{SL} due to the relatively large magnitude of ε_G. The P_AL effect diminishes at higher T values although an increase in the total emittance is still present. The interaction of scattering with gas emission diminishes for both Figs. 1 and 2 as κ_{SL} goes to zero since ε_S tends toward zero. Total emittance ε_T therefore approaches ε_G although, even for the smallest scattering optical depth investigated ($\kappa_{SL} = 0.001$), scattering is found to enhance the otherwise pure gaseous emission by a factor of approximately 1.7 or more. This trend toward ε_G is augmented by an increase in P_AL, a decline in T (increasing ε_G), or by increasing ω_S toward unity (decreasing ε_S).

Figure 2, the isopleth plot of ε_T for CO_2, exhibits trends very similar to those of H_2O. A slight drop in ε_T occurs only for the smallest scattering influence region (small κ_{SL} and large ω_S) as T increases from 300 to 1500 K for low P_AL. The total emittance is unchanged for those values greater than or equal to 0.2. This is to be compared to the value of 0.95 for H_2O. The values of ε_T larger than 0.4 are unchanged as T increases from 1500 to 3000 K. As noted for H_2O, an increase in P_AL intensifies the T effect and for $P_AL = 10.0$ atm m the effect of T alters the emittance as it does in Fig. A2. As T rises from 300 to 1500 K, ε_T is enhanced due to the maximum in the ε_G curves for CO_2. The total emittance declines for all κ_{SL} as T further increases to 3000 K with the effect being more pronounced at smaller ε_T isopleths. The P_AL effect follows the same trend in general as that for H_2O although, at $T = 1500$ K and $P_AL = 10.0$ atm m, the normally competing effects of T and P_AL now reinforce each other due to the change in local T effect, yielding a large net ε_T intensification. The magnitude of ε_T at $T = 3000$ K and large κ_{SL} are not affected by an increase in P_AL from 0.001 to 0.1 atm m,

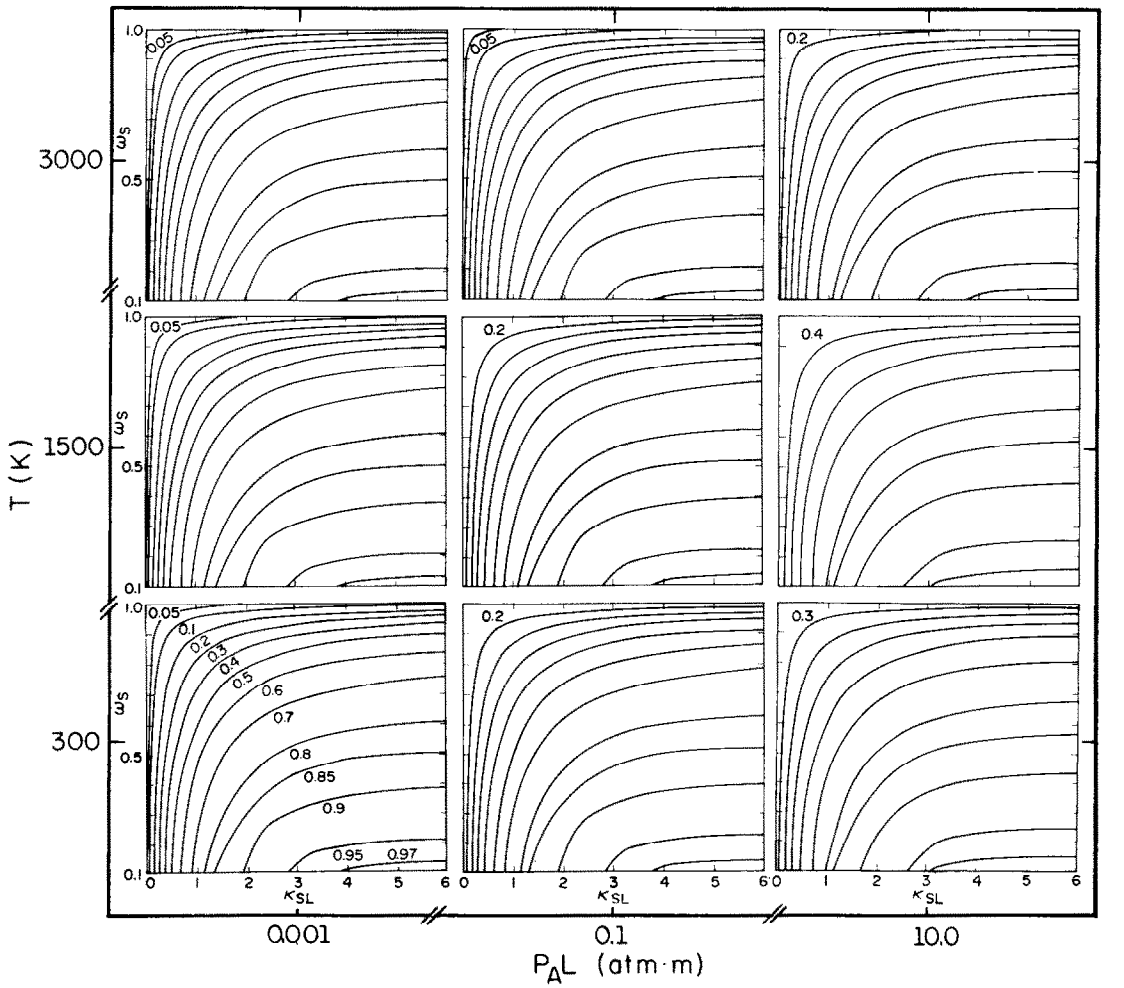

FIG. 2. Total hemispherical emittance isopleths for CO_2. Values increase from the indicated quantity in the order: 0.05, 0.1, 0.2, 0.3, 0.4, 0.5, 0.6, 0.7, 0.8, 0.85, 0.9, 0.95, 0.97.

yet ε_T values rise at all κ_{SL} for larger P_AL, reflecting the change in ε_G.

The effects of the scattering variables on ε_T suggest a division into conservative and nonconservative cases. For the nonconservative case as indicated above, ε_T diminishes as ω_S increases due to less gray emission (α_S is decreasing). This gray emission by the particulate phase dominates the emitted energy. Increasing ω_S results in longer possible path lengths but lower magnitudes for the path length distributions. (See ref. [11], noting the different definitions of optical depth.) The wide band absorption is a monotonically increasing function in length, which offsets the decrease in the path length distribution magnitudes, so that $\rho_{i^*}(\kappa_{SL}, \omega_S, \kappa_{HL}, \eta_b)$ and $\tau_{i^*}(\kappa_{SL}, \omega_S, \kappa_{HL}, \eta_b)$ increase with increasing ω_S. The diminution of the particulate phase emittance more than offsets the rise in the wide band emittance, resulting in a net decrease in ε_T.

Contrary to the total hemispherical emittance trends with respect to κ_{SL} discussed for the nonconservative case, ε_T declines as κ_{SL} rises for conservative scattering. The explicit exponential decay in equations (17) and (18) vanishes without gray absorption, and the result of the integration over λ can be interpreted in terms of a mean photon path length $\langle\lambda\rangle$ [18]. To better understand the discussion of the scattering-band absorption interaction, it is beneficial to recognize the κ_{SL} dependence of the optical path length distributions. As κ_{SL} increases, the quantity $\langle\lambda\rangle/\kappa_{SL}$ falls for $P(\lambda, \kappa_{SL})$ yet increases for $T(\lambda, \kappa_{SL})$, while the value of $P(\lambda, \kappa_{SL})$ remains on the same order of magnitude but the value of $T(\lambda, \kappa_{SL})$ drops greatly. [For example, the peak $T(\lambda, \kappa_{SL})$ value of about 2000 occurs at $\lambda = \kappa_{SL}$ for $\kappa_{SL} = 0.001$ compared to the peak $T(\lambda, \kappa_{SL})$ value of about 0.02 near $\lambda = \kappa_{SL}$ for $\kappa_{SL} = 5.0$.] Both distributions decay to zero at large λ, and as κ_{SL} increases the distributions broaden markedly in λ [11]. Since $\langle\lambda\rangle/\kappa_{SL}$ is large at small κ_{SL} for $P(\lambda, \kappa_{SL})$, the $A_{i^*}(\kappa_{HL}\lambda/\kappa_{SL}, \eta_b)$ magnitudes within the integration over λ in equation (17) are large. As κ_{SL} rises, the path length distributions become longer and lower in magnitude and the product of $A_{i^*}(\kappa_{HL}\lambda/\kappa_{SL}, \eta_b)$ and $P(\lambda, \kappa_{SL})$ lessens. As κ_{SL} increases, the rise in $\langle\lambda\rangle/\kappa_{SL}$ for $T(\lambda, \kappa_{SL})$, and thus the augmentation of $A_{i^*}(\kappa_{HL}\lambda/\kappa_{SL}, \eta_b)$, is more than offset by the drop in overall magnitude of $T(\lambda, \kappa_{SL})$. A net decrease in the product of $T(\lambda, \kappa_{SL})$ and $A_{i^*}(\kappa_{HL}\lambda/\kappa_{SL}, \eta_b)$ results. At best, $A_{i^*}(\kappa_{HL}\lambda/\kappa_{SL}, \eta_b)$ may only increase at a linear rate with respect to its first argument, thus $\rho_{i^*}(\kappa_{SL}, \omega_S, \kappa_{HL}, \eta_b)$, $\tau_{i^*}(\kappa_{SL}, \omega_S, \kappa_{HL}, \eta_b)$ and consequently ε_T decrease as κ_{SL} rises.

The total hemispherical emittance can be less than the pure gas emittance for the same T and P_AL due to the scattering path length and band absorptance interaction. For the conservative scattering case, the particulate phase only redistributes radiant energy and there is no emission by this phase. The increase in scattering optical depth to large values impedes the emission process of the layer. The 'shielding' effect is found to occur only for the conservative case at large P_AL and κ_{SL} values. The nonconservative case shows a marked ε_S increase as κ_{SL} rises so that a net enhancement in ε_T occurs. Physically, the possibility of longer path lengths amplifies the amount of absorption in the nonconservative layer, thereby increasing the emittance.

Charted results

The complexities of competing scattering and gaseous effects on the total emittance have been demonstrated. To diminish the complications somewhat and present ε_T in a more understandable manner, the parameter C as expressed in equation (24) is utilized. The parameter $C > 1$ can be thought of as the enhancement of gas emittance due to the presence of particulate, and $C < 1$ signifies the depletion of gas emittance due to scattering. The dependence of C on the four variables κ_{SL}, ω_S, T and P_AL, is shown in Appendix B and a discussion of the effects of the variables on the gas-scattering interaction is presented. It is shown that reasonable accuracy in the determination of the correction factor can be maintained by approximating the T effect linearly and the P_AL effect logarithmically between appropriate values. Figures 3–6 are to be used in conjunction with Figs. A1–A3 to determine approximate values of ε_T graphically.

A number of significant trends are present in Figs. 3 and 4. Scattering emittance becomes dominant as $(1-\omega_S)\kappa_{SL}$ increases and the effects of the gas parameters become negligible as all curves coalesce into a single curve. The upper curves begin to bend toward a unity correction factor as $(1-\omega_S)\kappa_{SL}$ approaches zero, and if smaller $(1-\omega_S)\kappa_{SL}$ values are examined all curves tend toward unity. The scatter of data points is due to the fact that $(1-\omega_S)\kappa_{SL}$ is not an exact scattering length scale for the entire ω_S and κ_{SL} domains presented [17].

The use of Figs. 3 and 4 requires the knowledge of T, P_AL, ω_S and κ_{SL} of a layer containing either H_2O or CO_2 gas. Once the appropriate ε_G and ε_S are read from Figs. A1–A3, the correction factor is obtained by locating P_AL between those presented for both $T = 300$ and 3000 K and performing a logarithmic interpolation in P_AL between the appropriate C values presented. A linear interpolation in T between the two C values just calculated yields the legitimate factor. The total emittance is thus given by equation (25). Using the figures provided and interpolation as indicated yields accuracies to within 5%. Extremely small ε_T values may yield slightly higher error percentages. Considering the expected accuracy of the exponential wide band model [5], these deviations are acceptable. For $(1-\omega_S)\kappa_{SL}$ values greater than those provided, approximating ε_T by ε_S is reasonable and for values of $(1-\omega_S)\kappa_{SL} > 5$, this approximation is within 5%.

The correction factor for conservative scattering, as displayed in Figs. 5 and 6, indicates; 'shielding' ($C < 1$) occurs at large P_AL and κ_{SL}, high P_AL eliminates any T effect, and $C \to 1$ as $\kappa_{SL} \to 0$. As κ_{SL} increases from moderate values, the total emittance decreases as noted

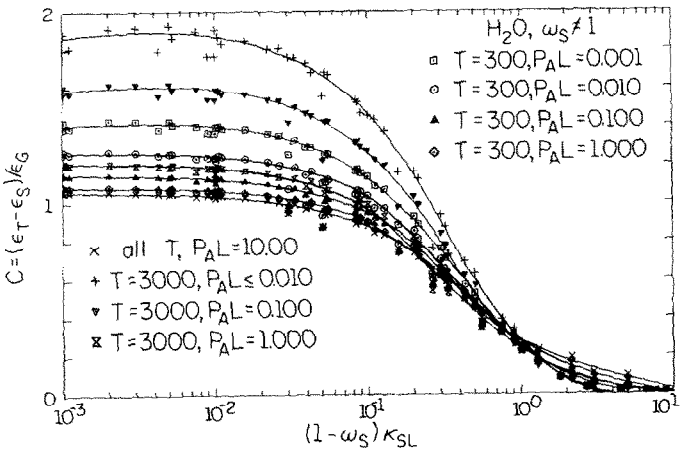

FIG. 3. The correction factor C for H_2O and nonconservative scattering. All references to P_AL and T values have units of atm m and K, respectively. Solid curves are a best fit approximation.

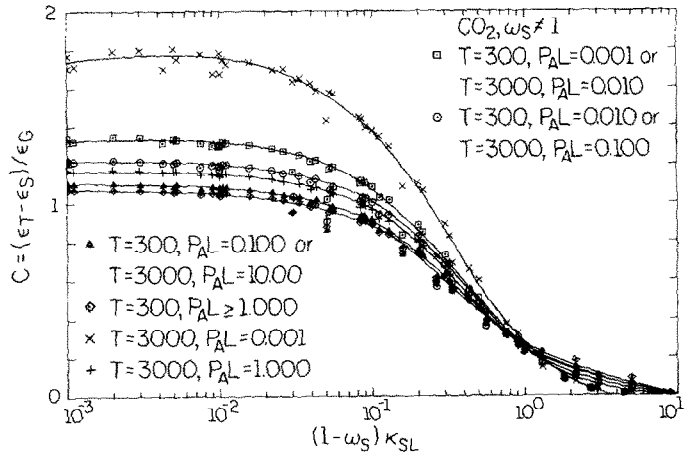

FIG. 4. The correction factor C for CO_2 and nonconservative scattering. All references to P_AL and T values have units of atm m and K, respectively. Solid curves are a best fit approximation.

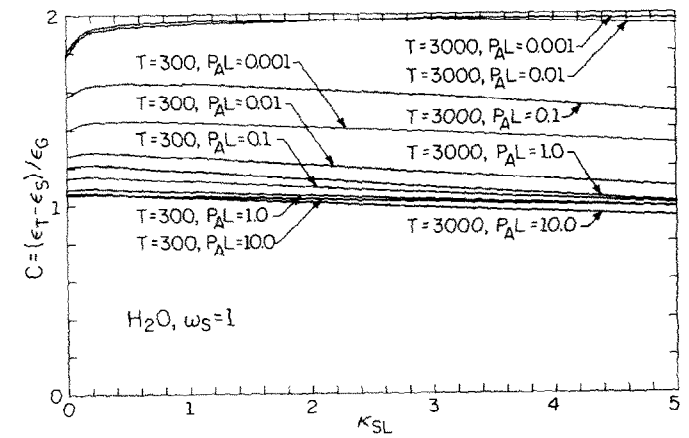

FIG. 5. The correction factor C for H_2O and conservative scattering. All references to P_AL and T values have units of atm m and K, respectively.

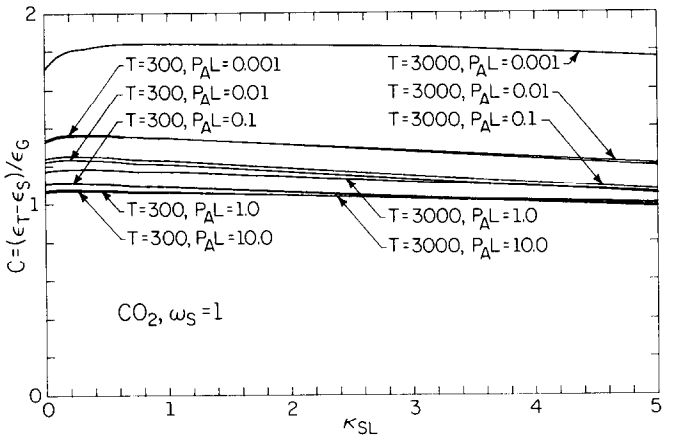

FIG. 6. The correction factor C for CO_2 and conservative scattering. All references to P_AL and T values have units of atm m and K, respectively.

in Appendix B except at low P_AL and high T, where ε_T is enhanced for H_2O only. The use of Figs. 5 and 6 is identical to that described for $\omega_S \neq 1$ with the exception that $\varepsilon_S(\kappa_{SL}, \omega_S = 1) = 0$. Similar accuracies can be expected.

The correction factor C, as presented in Figs. 3–6 for a total pressure of 1 atm, can be applied to situations which have other P_T values with slight additional error. Calculating the total emittance for nonunity total pressure by equation (25), using ε_G at the appropriate total pressure, yields results within 15% of the exact total emittance. The P_AL and P_T values tested are those in Hottel's pressure correction charts for gas emittance [1], although Hottel's pressure correction factor was not used. The partial pressure P_A was maintained at the zero limit and the remaining parameters spanned the domains previously identified. Average errors below 3% can be expected although extremely small total emittance values may yield slightly higher error percentages.

CONCLUSIONS

Total hemispherical emittance values for a medium containing a real gas and isotropically scattering particulate have been successfully determined by quantifying the gaseous absorption with the exponential wide band model, and incorporating the scattering effects through the optical path length approach. The exact method of analysis has been indicated and demonstrated. The technique only requires explicit integrations of known functions to yield results which can be considered extensions of Hottel's gas emittance charts to include scattering. An approximate graphical method of solution was presented utilizing the parameter

$$C = [\varepsilon_T(\kappa_{SL}, \omega_S, T, P_AL) - \varepsilon_S(\kappa_{SL}, \omega_S)]/\varepsilon_G(T, P_AL)$$

which was shown to be reasonably linear with respect to T and logarithmic in P_AL. A wide range of parameter values has been covered ($0.001 \leqslant P_AL\,[\text{atm m}] \leqslant 10.0$, $300 \leqslant T[\text{K}] \leqslant 3000$, $0.001 \leqslant (1-\omega_S)\kappa_{SL} \leqslant 10.0$ or $0.001 \leqslant \kappa_{SL} \leqslant 6.0$ for $\omega_S = 1$), for which an average error of 5% can be expected. Extremely small $\varepsilon_T(\kappa_{SL}, \omega_S, T, P_AL)$ values may yield slightly higher error percentages.

The total emittance values have been shown to be affected in numerous ways as a consequence of the gas-scattering interactions. Some of the more significant observations include:

(1) The inclusion of gray absorption by the particulate alters the gas-scattering interaction such that the $\omega_S = 1$ and $\omega_S \neq 1$ cases are significantly different.

(2) For the conservatively scattering case, scattering generally enhances the gas emittance except at large κ_{SL} and P_AL where $\varepsilon_T(\kappa_{SL}, \omega_S, T, P_AL)$ can be less than $\varepsilon_G(T, P_AL)$. As in the nonconservative case, the total emittance approaches pure gas emittance at large P_AL.

(3) The effect of a decrease in ω_S or a rise in κ_{SL} yields an increase in total emittance because $\varepsilon_S(\kappa_{SL}, \omega_S)$ rises more than $\varepsilon_{i*}(\kappa_{SL}, \omega_S, \kappa_{HL}, \eta_b)$ diminishes.

(4) The total emittance exhibits trends similar to pure gas emittance for high P_AL and low T values when $(1-\omega_S)\kappa_{SL}$ is small.

(5) Scattering emittance dominates the total emittance for large κ_{SL} and small ω_S, or large $(1-\omega_S)\kappa_{SL}$ values. $\varepsilon_T(\kappa_{SL}, \omega_S, T, P_AL)$ can be approximated by $\varepsilon_S(\kappa_{SL}, \omega_S)$ for all $(1-\omega_S)\kappa_{SL} > 5.0$ for either carbon dioxide or water vapor with an expected error below 5%.

Acknowledgement—This work was supported in part by the National Science Foundation under Grant No. MEA 81-09250.

REFERENCES

1. H. C. Hottel, in *Heat Transmission* (3rd edn.), (by W. H. McAdams), Chap. 4. McGraw-Hill, New York (1954).
2. R. M. Goody, *Atmospheric Radiation—I. Theoretical Basis*, p. 153. Oxford University Press, London (1964).
3. T. F. Smith and Z. F. Shen, Evaluation of coefficients for

the weighted sum of gray gases model, ASME Paper No. 81-HT-55, 20th National Heat Transfer Conference, Milwaukee, Wisconsin, April (1981).
4. D. K. Edwards, Molecular gas band radiation, *Adv. Heat Transfer* **12,** 115–193 (1976).
5. D. K. Edwards and A. Balakrishnan, Thermal radiation by combustion gases, *Int. J. Heat Mass Transfer* **16,** 25–40 (1973).
6. A. L. Crosbie, Apparent radiative properties of an isotropically scattering medium on a diffuse substrate, *J. Heat Transfer* **101,** 68–75 (1979).
7. A. Dayan and C. L. Tien, Radiative transfer with anisotropic scattering in an isothermal slab, *J. Quantve Spectros. Radiat. Transfer* **16,** 113–125 (1976).
8. P. B. Taylor and P. J. Foster, The total emissivities of luminous and non-luminous flames, *Int. J. Heat Mass Transfer* **17,** 1591–1605 (1974).
9. J. D. Felske and C. L. Tien, Calculation of the emissivity of luminous flames, *Combust. Sc. Tech.* **7,** 25–31 (1973).
10. C. L. Tien and S. C. Lee, Flame radiation, *Prog. Energy Combust. Sci.* **8,** 41–59 (1982).
11. R. D. Skocypec and R. O. Buckius, Photon path length distributions for an isotropically scattering planar medium, *J. Quantve Spectros. Radiat. Transfer* **28,** 425–439 (1982).
12. H. Lee and R. O. Buckius, Scaling anisotropic scattering in radiation heat transfer for a planar medium, *J. Heat Transfer* **104,** 68–75 (1982).
13. R. O. Buckius, The effect of molecular gas absorption on radiative heat transfer with scattering, *J. Heat Transfer* **104,** 580–586 (1982).
14. R. O. Buckius and A. Fernandez-Fraga, The optical path length approach to radiation heat transfer with isotropic scattering and gaseous absorption, *J. Quantve Spectros. Radiat. Transfer* **24,** 1–13 (1980).
15. A. T. Modak, Exponential wide band parameters for the pure rotational band of water vapor, *J. Quantve Spectros. Radiat. Transfer* **21,** 131–142 (1979).
16. J. D. Felske and C. L. Tien, A theoretical closed form expression for the total band absorptance of infrared-radiating gases, *Int. J. Heat Mass Transfer* **17,** 155–158 (1974).
17. H. Lee and R. O. Buckius, Reducing scattering to nonscattering problems in radiation heat transfer. *Int. J. Heat Mass Transfer* **26,** 1055–1062 (1983).
18. R. O. Buckius, Radiation heat transfer using mean photon path lengths, *Int. J. Heat Mass Transfer* **25,** 917–923 (1982).

APPENDIX A

PURE GAS AND PURE SCATTERING EMITTANCE

(See Figs. A1–A3.)

APPENDIX B

THE EFFECT OF GAS AND SCATTERING VARIABLES ON THE CORRECTION FACTOR C

The explicit temperature dependence of C is presented in Figs. B1(a) and (b). Figure B1(a) demonstrates a number of interesting effects for conservative scattering. Scattering generally enhances the gas emittance except at large κ_{SL} and P_AL, where the 'shielding' phenomenon occurs (noted by $C < 1$). The enhancement ($C > 1$) is amplified at low P_AL since both $\varepsilon_G(T, P_AL)$ and the effective gas optical depth are small, so that any amount of scattering increases them significantly. The wide band absorptances are low at small P_AL yielding small gas emittance values. However, the magnitude of $A_{i*}(\kappa_{HL}\lambda/\kappa_{SL}, \eta_b)$ can rise greatly as λ increases within the integrand of equations (17) and (18). An increase in T further lowers the wide band absorptance and additionally augments the scattering enhancement. The crossover for low P_AL is due to the rate of increase of $A_{i*}(\kappa_{HL}\lambda/\kappa_{SL}, \eta_b)$ relative to the decay rate of the path length distributions as λ becomes longer. The integrand product of the linearly increasing $A_{i*}(\kappa_{HL}\lambda/\kappa_{SL}, \eta_b)$ and $P(\lambda, \kappa_{SL})$ or $T(\lambda, \kappa_{SL})$ is larger for large κ_{SL} as T increases. This is not seen for larger P_AL values because the rate of increase of $A_{i*}(\kappa_{HL}\lambda/\kappa_{SL}, \eta_b)$ with λ lessens toward the log or square root region. The correction factor is constant with respect to T and tends toward unity for large P_AL because $\varepsilon_G(T, P_AL)$ dominates $\varepsilon_T(\kappa_{SL}, \omega_S, T, P_AL)$ and both have the same T dependence.

Figure B1(b) presents the correction factor for the nonconservative case as a function of the group $(1-\omega_S)\kappa_{SL}$, or $\alpha_S L$, since it is the appropriate approximate scattering length scale [17]. The scaling is valid only for the nonconservative case because not only are the physics of the $\omega_S = 1$ and $\omega_S \neq 1$ cases different, but the lower limit of the scaling does not agree for both cases. As $(1-\omega_S)\kappa_{SL}$ increases, C values diminish toward zero for all T since $\varepsilon_S(\kappa_{SL}, \omega_S)$ becomes more dominant. Similar to the conservative case discussed above, small P_AL results retain the gaseous characteristics as indicated by the effect of T, while exhibiting no T effect at high P_AL. There is little effect of P_AL on C as $(1-\omega_S)\kappa_{SL}$ increases toward unity.

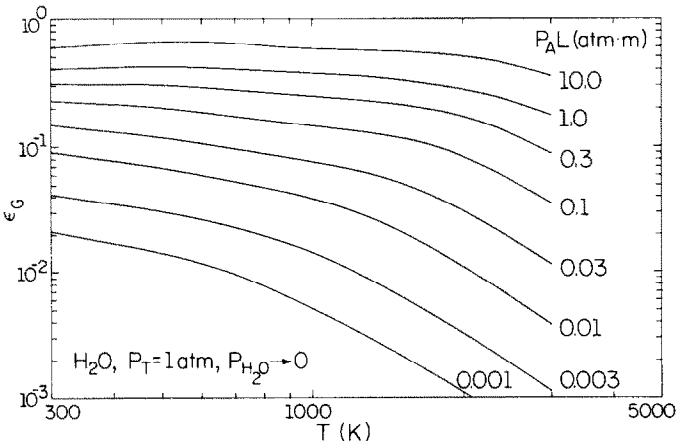

FIG. A1. Total hemispherical pure gas emittance for H_2O.

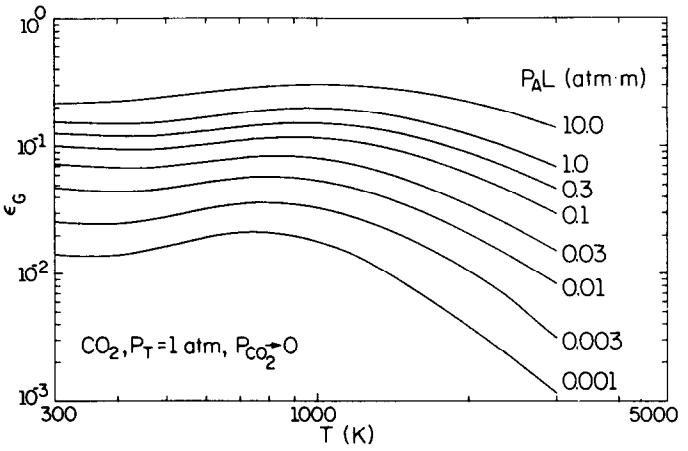

FIG. A2. Total hemispherical pure gas emittance for CO_2.

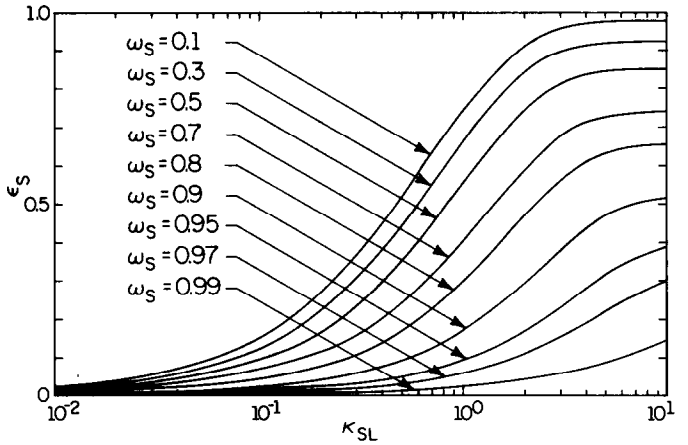

FIG. A3. Total hemispherical particulate emittance with isotropic scattering.

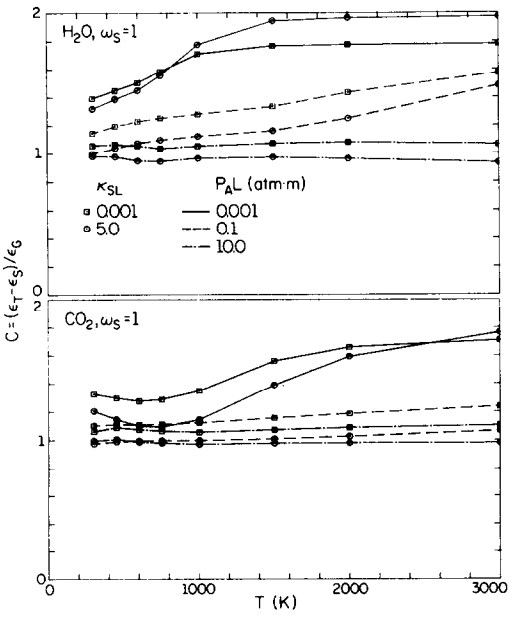

FIG. B1(a). The effect of temperature on the correction factor C for conservative scattering.

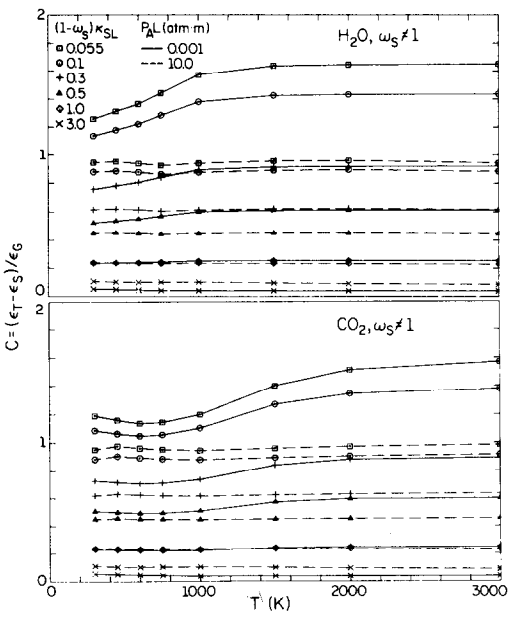

FIG. B1(b). The effect of temperature on the correction factor C for nonconservative scattering.

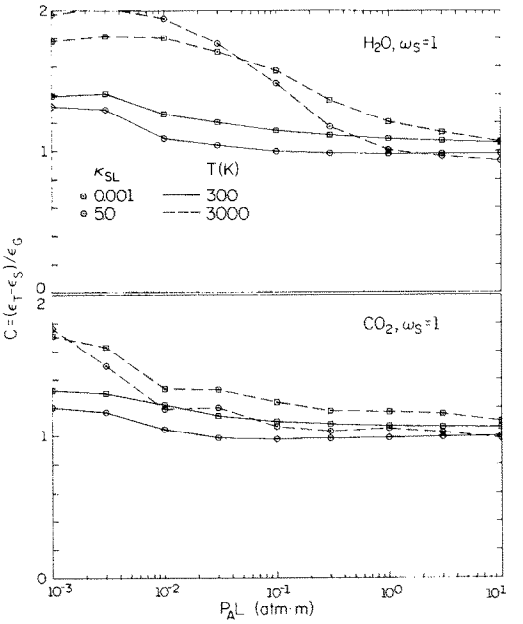

FIG. B2(a). The effect of the partial pressure and path length product on the correction factor C for conservative scattering.

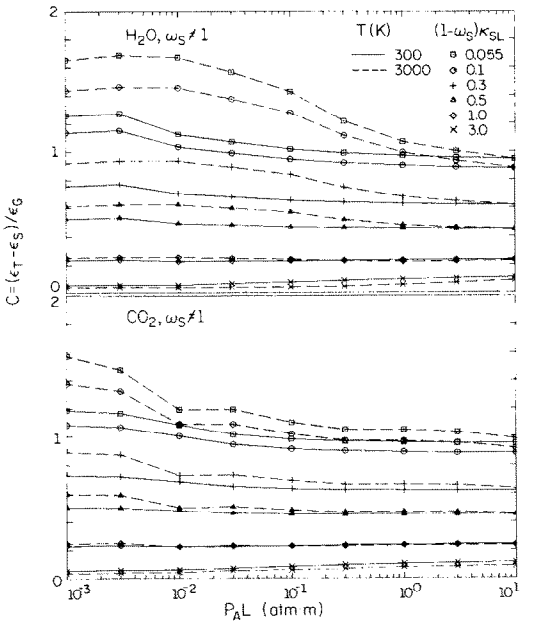

FIG. B2(b). The effect of the partial pressure and path length product on the correction factor C for nonconservative scattering.

For small $(1-\omega_S)\kappa_{SL}$, a reduction in P_AL renders an increase in C until $(1-\omega_S)\kappa_{SL}=1$ where no P_AL effect is noted. Further increases in the length scale yield a decrease in C for a reduction in P_AL. The cause of the reversal is believed to be due to higher orders of scattering forcing $T(\lambda, \omega_S\kappa_{SL})$ to peak at λ values greater than κ_{SL}, which is the peak location in λ for smaller κ_{SL}. The exponential decay factor plays a large role since the reversal is not apparent for the conservative case. A reasonable linear approximation for the effect of T on the correction factor is made, cognizant that nonlinearity occurs at small P_AL and T.

A more detailed view of the correction factor in terms of P_AL is shown in Figs. B2(a) and (b). One new phenomenon is shown in Fig. B2(a) in addition to previously identified trends. At low P_AL and high T, the smallest κ_{HL} occurs and the effect of κ_{SL} crosses, indicating how the smallest $A_i*(\kappa_{HL}\lambda/\kappa_{SL}, \eta_b)$ values interact differently with the path length distributions. Figure B2(b) for the nonconservative case exhibits the trends previously noted for Fig. B1(b). Logarithmic interpolation between appropriate P_AL values is a plausible approximation, especially for high $(1-\omega_S)\kappa_{SL}$ and P_AL.

EMITTANCES HEMISPHERIQUES TOTALES POUR CO_2 ET H_2O INCLUANT LA DIFFUSION PARTICULAIRE

Résumé—On détermine l'émittance hémisphérique totale d'une couche plane contenant un gaz spectralement absorbant et à diffusion isotrope particulaire. Le modèle de bande exponentiel est utilisé pour représenter l'absorption gazeuse tandis que le concept d'épaisseur optique est employé pour inclure les effets de la diffusion. Les valeurs d'émittance totale pour la vapeur d'eau ou le dioxyde de carbone avec des particules sont présentées. De nombreux effets interactifs gaz-diffusion et des effets variables sont identifiés et expliqués. Une solution technique est présentée qui fournit sans calculs les valeurs approchées mais assez précises de l'émittance totale.

HALBRAUMSTRAHLUNG VON CO_2 UND H_2O BEI TEILWEISER STREUUNG

Zusammenfassung—Es wird die Gesamtemission in den Halbraum von einer ebenen Schicht untersucht, welche ein spektral absorbierendes Gas und isotrop streuende Partikel enthält. Die Absorption im Gas wird mit dem exponentiellen Breitbandmodell beschrieben und die Einflüsse der Streuung nach dem Konzept der optischen Weglängen behandelt. Es werden die Gesamtwerte für die Emission von Wasserdampf und Kohlendioxid mit Streuung an Partikeln angegeben. Zahlreiche Wechselwirkungen zwischen Gasabsorption und Streuung sowie unabhängige Einfüsse werden festgestellt und erklärt. Mit einer tabellarischen Lösungsmethode lassen sich nahezu genaue Gesamtemissionswerte ohne Berechnung bestimmen.

ОПРЕДЕЛЕНИЕ СУММАРНОЙ ПОЛУСФЕРИЧЕСКОЙ ЛУЧЕИСПУСКАТЕЛЬНОЙ СПОСОБНОСТИ CO_2 И H_2O С УЧЕТОМ РАССЕЯНИЯ НА МАКРОЧАСТИЦАХ

Аннотация—Определена суммарная полусферическая лучеиспускательная способность плоского слоя, содержащего спектрально поглощающий газ и изотропно рассеивающие макрочастицы. Для определения поглощения газовой фазой используется экспоненциальная широкополосная модель, а приближение длины оптического пути используется для учета эффектов рассеяния. Представлены суммарные значения лучеиспускательной способности водяного пара и углекислого газа, содержащих макрочастицы. Определены различные эффекты взаимодействий в рассеивающем газе и дано их объяснение. Представлен графический метод решения, позволяющий, не прибегая к расчетам, получать приближенные, но вполне удовлетворительные, значения суммарных коэффициентов лучеиспускания.